51st AIAA Aerospace Sciences Meeting including the New Horizons Forum and Aerospace Exposition
07 - 10 January 2013, Grapevine (Dallas/Ft. Worth Region), Texas

AIAA 2013-0391

Measurements of the Interaction of an Upstream Laser Perturbation with a Forward-Facing Cavity

Amanda Chou*, Steven P. Schneider†, and Steven H. Collicott†
School of Aeronautics & Astronautics, Purdue University, West Lafayette, IN 47907, USA

The laser perturber is a tool to be used for receptivity studies in the Boeing/AFOSR Mach-6 Quiet Tunnel. To demonstrate that the laser perturber is functioning correctly, it is tested with a forward-facing cavity. Results are similar to previous studies by Ladoon and Segura in a Mach-4 quiet tunnel. The cavity base pressure fluctuations are nearly quiescent at shallow cavity depths. When a freestream perturbation interacts with the forward facing cavity, the cavity base pressure experiences oscillations that decay exponentially. The measured cavity resonance frequency matches the theoretical cavity resonance frequency to within 6%. The measured cavity response appears to be initiated by the acoustic disturbance that results from the laser-generated perturbation. The damping characteristics of the forward-facing cavity are also examined. For cavities with similar resonant frequencies, the damping constants can differ by almost an order of magnitude. However, cavities with similar non-dimensional depths have similar damping constants.

Nomenclature

D	cavity diameter, mm
E_{pulse}	laser energy per pulse, mJ
f_1	fundamental cavity resonance frequency, kHz
L	cavity depth, mm
M	Mach number
p	pressure, kPa
Re	Reynolds number
T	temperature, °C or K
y	spanwise tunnel coordinate ($y = 0$ on tunnel centerline), mm
z	axial tunnel coordinate ($z = 0$ at throat), m
Δz	distance between model nose and perturbation
δ	mean bow shock standoff distance, mm
$\gamma/2$	cavity resonance damping coefficient, rad/s
μ	Mach angle
ω_1	fundamental angular frequency, rad/s

Subscript

0	at stagnation conditions
1	conditions before a shock
2	conditions after a shock
i	at initial conditions
AO	acoustic origin
n	natural/computed condition
nose	at the nose
pulse	of the laser pulse
r	response (signal reaches 10% of maximum)

Superscript

$'$	RMS fluctuations

Abbreviations

BAM6QT	Boeing/AFOSR Mach-6 Quiet Tunnel
Nd:YAG	Neodymium-doped Yttrium-Aluminum-Garnet crystal
PQFLT	Purdue Quiet Flow Ludwieg Tube (Mach-4 Tunnel)
RMS	root-mean-square

I. Introduction

Transition in the hypersonic regime is not a well-understood process. In order to study this phenomenon, more experimental research is needed. Flight tests usually cost orders of magnitude more than ground tests,

*Graduate student, AIAA Student Member
†Professor, AIAA Associate Fellow.

so experiments are typically conducted in wind tunnels. Unfortunately, no single wind tunnel is capable of simulating all aspects of flight, so many different wind tunnels must be used to understand the intricacies of the transition process.

One such aspect is the effect of freestream noise on transition. Conventional tunnels have turbulent nozzle-wall boundary layers which radiate acoustic noise into the freestream. The noise level in conventional tunnels is orders of magnitude greater than the freestream noise in flight. Quiet tunnels, which were developed by the NASA Langley Research Center (LaRC) from the 1960s to the 1990s, are tunnels with laminar nozzle-wall boundary layers.[1] They provide freestream pressure fluctuation conditions that are similar to those in flight, which affects transition location.[2]

Receptivity, the way in which disturbances in the freestream enter the boundary layer, is a particular part of transition that is not understood. The freestream disturbance must typically pass through a shock wave, whose effect on the initial amplitude of instabilities in the boundary layer is unknown. This creates critical problems in our understanding of the physics of flow in the hypersonic regime. A better understanding of receptivity at hypersonic speeds can help to develop amplitude-based models for transition. Without an understanding of the basic physics and good models for transition, the design of hypersonic vehicles such as re-entry vehicles can be flawed. These flaws contribute to under-design of a vehicle, such as too little thermal protection, which can result in catastrophic failure. To compensate, designers may be inclined to over-design a vehicle, which can result in unnecessary cost or make it unfeasible to achieve a mission.

II. The Boeing/AFOSR Mach-6 Quiet Tunnel

The Boeing/AFOSR Mach-6 Quiet Tunnel (BAM6QT) is currently one of two operational hypersonic quiet tunnels in the world (Figure 1). It is the only known hypersonic quiet tunnel with optical access far upstream. The tunnel is a Ludwieg tube with a valve downstream of the test section, so models and instrumentation must be able to withstand the full stagnation pressure. This valve consists of a set of two burst diaphragms. Several features are used to keep laminar boundary layers on the nozzle wall. Filters to reduce particles in the freestream are used to minimize the likelihood of particle impact. A mirror-finish polish on the nozzle wall helps to reduce the likelihood of roughness-induced transition. The nozzle is also longer than that of a conventional tunnel to minimize the likelihood of transition due to the Görtler instability. Just upstream of the throat, a bleed valve suctions off the air, allowing a fresh boundary layer to grow along the length of the nozzle. To run this tunnel in a conventional or "noisy" configuration, the bleed valve is closed to allow the boundary layer to develop naturally.

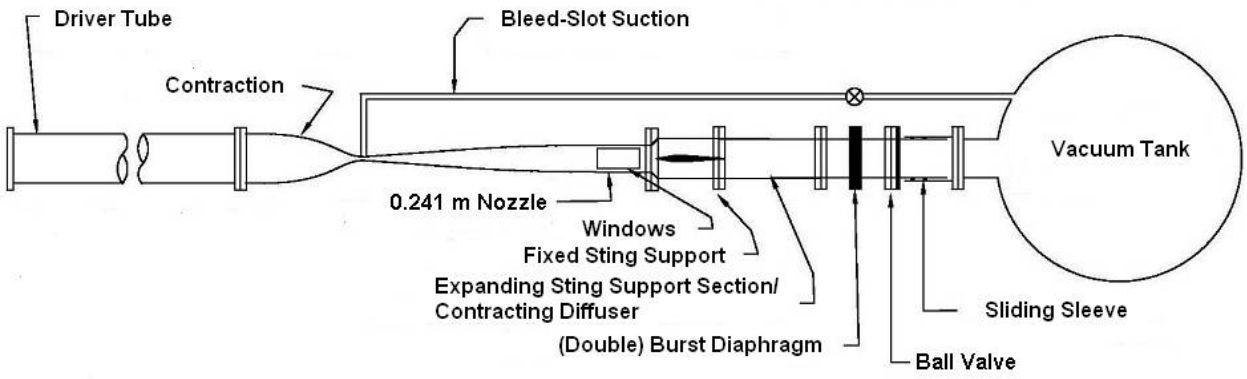

Figure 1. A schematic of the Boeing/AFOSR Mach-6 Quiet Tunnel.

III. Laser Perturber

The purpose of the laser perturber apparatus is to create a well-controlled, repeatable perturbation in the freestream of a wind tunnel. This perturbation must be large enough and simple enough to characterize, but

also small enough that it does not induce bypass transition. The simplicity of this type of freestream perturbation is especially useful for comparing to theory or computations. Since the structure of the perturbation is fairly straightforward, it can be easily modeled and incorporated into computations.

Laser-induced breakdown of air generates a disturbance in the freestream. The laser-generated perturbation consists of both an acoustic and an entropic (thermal) disturbance. The thermal/entropic disturbance makes up the core of the perturbation and should convect at the flow speed.[3] The acoustic disturbance emanates from this thermal core and travels at the speed of sound relative to the thermal disturbance in all directions. The acoustic disturbance is expected to decay fairly rapidly, leaving the thermal disturbance to be the primary disturbance used for receptivity studies. This thermal disturbance should essentially appear as a pulse.[4,5]

The laser perturber system consists of a high-powered laser and a lens system which focuses the laser beam inside the BAM6QT. The laser used is a Spectra-Physics Quanta-Ray GCR-190-10. It is a frequency-doubled (532 nm) Nd:YAG laser that pulses at 10 Hz. Each pulse has a width of about 7 ns and is capable of a maximum energy of about 310 mJ. To increase the shot-to-shot repeatability of the laser, a Spectra-Physics model 6350 seeder is used. The spatial profile of the beam also has a 90% Gaussian fit.

The optical system was designed by Collicott using ZEMAX[6] and consists of three air-spaced YAG triplets manufactured by CVI Melles Griot (Figure 2). The lenses in the system are

- a YAN-50.0-10.0 (negative effective focal length) used to expand the laser beam
- a YAP-200.0-40.0 (positive effective focal length) used to collimate the laser beam
- a YAP-200.0-40.0 (positive effective focal length) used to focus the laser beam

The beam passes through a flat 38.1-mm-diameter window of 46.6-mm thickness after the last lens. Using ZEMAX, the RMS radius is found to be 1.251 μm and the Airy (diffraction-limited) radius is 3.979 μm.

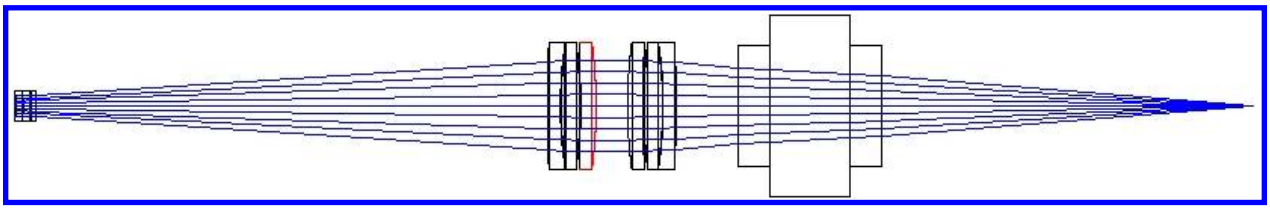

Figure 2. Laser perturber optical system schematic. Laser beam direction from left to right.

A. Effect of Window Shapes on Freestream Noise

Custom windows for this project were designed by Metrolaser and DEI and manufactured by B-Con Engineering in 2002.[7–9] The window mounted in the BAM6QT is centered at an axial location of $z = 1.924$ m, where $z = 0$ is the location of the throat. Both contoured and flat windows were manufactured. However, at present, the optical system for the laser perturber has only been made to work with the flat window.[10]

Since the window used is flat and the BAM6QT test section is axisymmetric, there may be some aerodynamic effects from this window. Preliminary tests to determine if this window affects the noise in the tunnel were conducted with a pitot-mounted Kulite probe. The Kulite probe was a mechanically-stopped, B-screen XCQ-062-15A. Three types of windows were examined: a stainless-steel contoured blank, a custom-ground contoured window, and a flat window (used to create laser-generated perturbations).

An assumption that the tunnel is of constant diameter is used to correlate the acoustic origin of the noise to the vertical measurement position. The acoustic origin is the location from which noise is radiated to a measurement location. It is estimated by tracing a Mach line from the measurement location to the closest wall. The axial location of the acoustic origin is approximated as

$$z_{AO} = z_{\text{probe}} - \frac{R - y}{\tan \mu} \tag{1}$$

where z_{probe} is the axial location of the probe with respect to the throat, R is the assumed-constant radius of the tunnel, y is the probe's distance from the tunnel centerline, and μ is the assumed-constant Mach angle.

Figure 3 shows the Mach number inferred from Kulite measurements of stagnation pressure across the test section. The gray shaded area shows the region of measurement locations corresponding to the acoustic origin of the sleeve in which the window glass is mounted. This area also represents the edges of the stainless steel blank. The blue shaded area shows the measurement location corresponding to the acoustic origin of the window glass. The Mach number is calculated numerically using a Newton-Raphson method with the measured total pressure ($p_{0,2}$) and the measured stagnation pressure of the driver tube ($p_{0,1}$). Measurements with the stainless-steel blank in the nozzle wall (filled black circles) and the contoured window (blue open circles) both show a fairly constant Mach number across the test section.

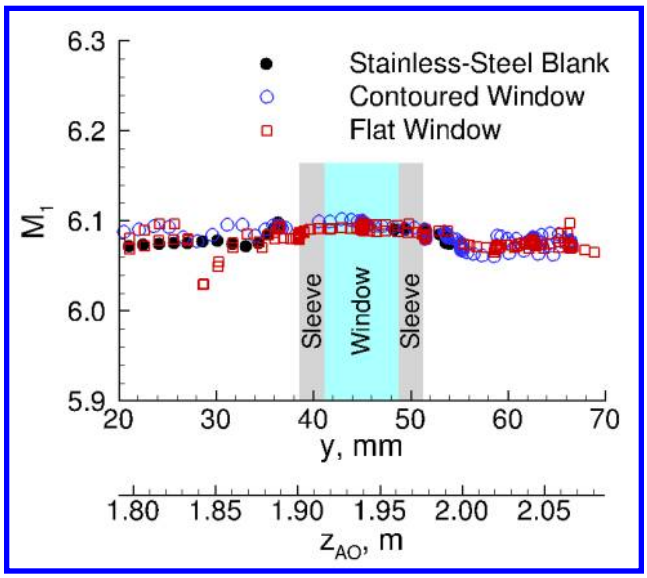

Figure 3. Measured Mach number across the test section for different windows and blanks.

Measurements taken with the flat window mounted in the nozzle wall (red squares) show a slight dip in Mach number at a measurement position of about 30 mm above the centerline of the tunnel. Two separate surveys across this region confirm the dip in Mach number. However, this dip does not appear to correspond with the window edges or sleeves. This is because the acoustic origin approximation assumes a one-dimensional, inviscid flow. Furthermore, the changing radius of the expanding nozzle is not taken into account. Measurements at this location are given by a fairly coarse survey. Further tests need to be conducted to better measure the location of the Mach wave that results from the junction of the flat window and the tunnel wall.

To determine the effect of this Mach wave, the noise level across the test section was also measured. The noise level measured at different vertical positions at $z = 2.374$ m and an initial stagnation pressure of $p_{0,i} \approx 1100$ kPa are shown in Figure 4. At each location, the probe pauses for 0.3 seconds, so there are fewer data points than in Figure 3. As expected, the stainless-steel blank shows a low, nearly-constant noise level, regardless of measurement location. For both windows, the noise level is higher for a measurement location that corresponds to an acoustic origin downstream of the window location. This was expected for the flat window, but not for the contoured window. It is possible that there is a bad seal around the contoured window which could create an jet on the nozzle wall during a run. It is also possible that this increase in noise is due to a shimmering Mach wave. However, this increase in noise does not exceed the quiet flow limit of 0.06%[11] for either window.

IV. Forward-Facing Cavity

Forward-facing cavities are geometries used as a form of passive heat transfer reduction at the nosetip of a blunt body, such as an optically-guided interceptor missile.[12,13] However, these forward-facing cavities resonate. Cavity resonance causes the bow shock in front of the nose to oscillate, which creates an unsteady flowfield. This bow shock oscillation can be stable, which means that the shock is symmetric about the nose and the oscillations are small. In some experiments, the bow shock becomes unstable. When the bow shock

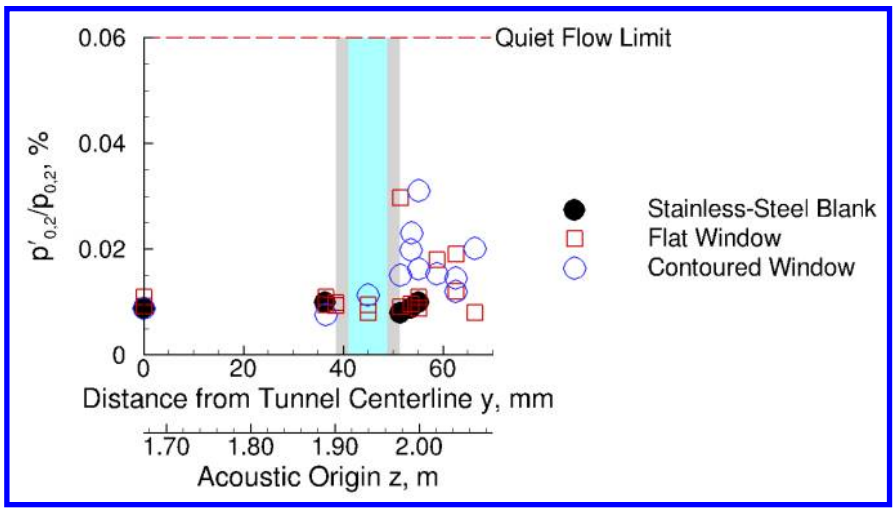

Figure 4. Noise measurements showing effects of different window inserts.

is unstable, the shock does not oscillate in a controlled manner and the oscillation amplitudes are large.[13–15] Under quiet flow, shallow cavities are almost quiescent, which explains the low heat transfer level seen in flight.[12] However, deeper cavities undergo self-sustained oscillations, even in quiet flow.

A forward-facing cavity (Figure 5) is used in the BAM6QT to prove that the laser perturber can create a measurable and controlled freestream disturbance. The physical response of the model is fairly well-known from previous experiments in the Mach-4 Purdue Quiet Flow Ludwieg Tube (PQFLT).[16–18] Computations have also been done on similar geometries by Engblom.[12] The response of this model without the presence of forced freestream perturbations at Mach 6 was presented in Reference 19.

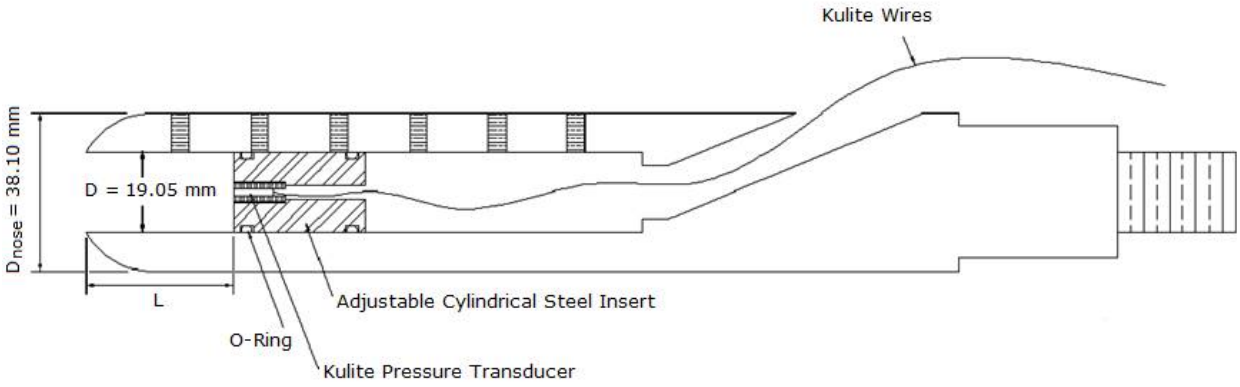

Figure 5. Schematic of forward-facing cavity model.

A. Background

The forward-facing cavity acts as a resonance tube, where the pressure fluctuations within the cavity have a dominant fundamental frequency of

$$\omega_{1n} = 2\pi f_{1n} = \frac{\pi a_0}{2L^*} \tag{2}$$

where a_0 is the speed of sound based on stagnation temperature in the cavity and $L^* = L + \delta$ is the axial distance between the cavity base and mean shock location. The mean shock standoff distance δ can be estimated using existing correlations. However, no correlation currently exists for a forward-facing cavity. The shock standoff distance was approximated by averaging the correlation for that of a flat-nosed cylinder

and that of a sphere. Similar approximations were used by Ladoon[16] and Segura.[17,18] At $M = 6$, $\delta = 0.54D$ for a flat-nosed cylinder and $\delta = 0.14D$ for a sphere.[20] The average of these two expressions gives $\delta = 0.34\,D$ for the forward-facing cavity. The constant D is as noted in Figure 5.

At some critical depth, a forward-facing cavity becomes unstable and creates self-sustained resonance, even under quiet flow. Previous tests under quiet flow show that the pressure fluctuations within a deep, unstable cavity are almost three orders of magnitude larger than when the cavity depth is shallow.[19] Ladoon was unable to find the critical depth at Mach 4 using only the freestream noise in the PQFLT because his model could only produce shallow cavities. Almost 10 years later, Segura designed another model with a deeper cavity and found that the critical cavity depth was about $L/D = 1.2$ using only the freestream noise in the Mach-4 tunnel.[17,18] Previous tests by the present author at Mach 6 showed that the critical cavity depth is also $L/D = 1.2$ for a larger model and higher Mach number.[19]

Ladoon used the damping characteristics of the cavity response to a laser-induced perturbation to extrapolate to the critical depth. This can be done by assuming that the response produces a damped sinusoid with an exponential envelope of the form

$$p'_{02} = C \exp\left[-\frac{\gamma}{2}t\right] \tag{3}$$

where p'_{02} is the RMS pressure fluctuation at the base of the cavity, C is some constant with units of pressure, $\gamma/2$ is the decay rate, and t is the time after excitation. Ladoon then used a least-squares method to fit exponential envelopes to the peaks of the response of a forward-facing cavity. Ladoon found that the exponential envelope decay rate ($\gamma/2$) could be correlated to the fundamental cavity resonance frequency (ω_1). Using a power-law fit, the correlation was found to be

$$\frac{\gamma}{2} = 1.0273 \times 10^{-12}\,\omega_1^{3.227} \tag{4}$$

where $\gamma/2$ and ω_1 have units of radians per second.[16]

This damping constant $\gamma/2$ can also be associated with the cavity depth using Equation 2. Ladoon used the data point with smallest $\gamma/2$ and the slope of Equation 4 at that point to linearly extrapolate when $\gamma/2 = 0$. This corresponded to a critical angular frequency ($\omega_{1,\text{critical}}$) of 18,200 rad/sec, which corresponds to $(L/D) = 2.7$.[16]

B. Model Positioning

In the BAM6QT, the nominal onset of uniform flow on the centerline occurs near $z = 1.914$ m.[21] The laser perturbation is created at a location of $z = 1.925$ m. The location of this perturbation is limited by the optical design of the perturber as well as the optical access into the tunnel. The perturber optics were aligned with a slight angle between the window and the perturber optics. This was done to reduce the risk of damage from back reflections of high-energy laser light.

The large-diameter nose facilitates the alignment of this model with the freestream laser perturbation. Some issues with alignment were discussed in Reference 10. Some improvements to the alignment process have been incorporated in the measurements presented in this paper. The current alignment procedure uses a digital level to measure the pitch angle of the model with respect to the tunnel centerline. The perturbation is aligned to the model with a straight toothpick mounted in the center of the cavity. For the alignment process, the sting is secured to be parallel within 0.1° to the tunnel centerline with a digital protractor. The optics and the model are adjusted until the tip of the toothpick is burned by the focused laser light. When the tip of the toothpick is burned, the focus of the system has been found and aligned with the centerline of the model. The sting is then moved along the tunnel centerline through the sting mount until the axial position of the model is as desired. The sting is again aligned so that the pitch is within 0.1° of the tunnel centerline. There may still be some uncertainty in the yaw of the model.

The farthest forward location tested did not require changing the axial position of the model after alignment with the laser-generated perturbation. This position is similar to the distance between the model and perturbation in the PQFLT. However, when the model is placed at this far-forward location in the BAM6QT, the model may no longer be in uniform flow, as shown in Figure 6. This was not the case for Ladoon's experiments, where the entire nose of the model was in uniform flow.[16] At the farthest-forward location tested in the BAM6QT, the nose of the model is at about $z = 1.98$ m. However, since the onset of uniform flow occurs at $z = 1.914$ m and the Mach angle at that location is about 9.6°, it is likely that parts of the model are not in uniform flow.

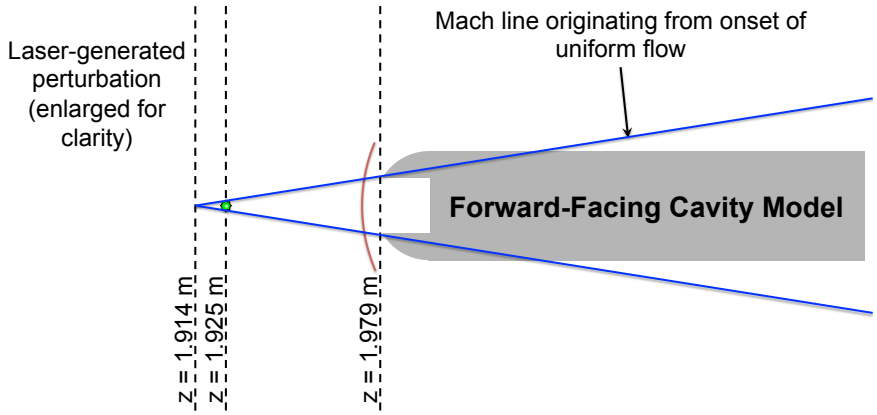

Figure 6. Diagram of axial location of model in the tunnel. All items to scale, except perturbation.

C. Instrumentation

The model used for the Mach-6 experiments (Figure 5) was designed by Segura in 2008.[17,18] The maximum L/D possible for this model is 5.00. The depth was varied by sliding the cylindrical steel insert back and forth and held constant by tightening set screws on the side of the model. The cavity is sealed at the base using two o-rings on the cylindrical steel insert. For laser perturber tests, L/D is varied only over 0–1.00 due to the observation of self-sustained resonance at conditions as low as $L/D = 1.15$. An exponential decay in perturbation-induced resonance is not seen when self-sustained resonance occurs.

Pressure fluctuations in the cavity were measured with a B-screen Kulite XCQ-062-15A pressure transducer mounted in the base of the cavity, within the cylindrical steel insert. These sensors are mechanically stopped at pressures above 15 psia to prevent damage to the transducer. The particular sensor used in this experiment has a resonant frequency of about 270 kHz. These Kulite transducer screens provide better protection against particle impact, as compared to the A-screen model, but are reported to have decreased frequency response. This limitation should not be a problem for forward-facing cavity experiments because the fundamental cavity resonance frequency is less than 20 kHz.

Previous tests with no forced freestream perturbations are discussed in Reference 19. All data presented in this paper has a freestream perturbation located at $z = 1.925$ m, upstream of the forward-facing cavity. Each of these perturbations is made with the optical equipment discussed in Section III. The laser energy is reduced by a beam sampler to 140-180 mJ/pulse near the BAM6QT windows.

Data were acquired using two Tektronix DPO7054 Digital Phosphor Oscilloscopes. These oscilloscopes have an 8-bit vertical resolution. Using the "Hi-Res mode" allows for the vertical resolution to be digitally increased to over 11 bits. This mode allows the oscilloscope to take data at the maximum sampling rate and to average the data in real time. Data is saved at the sampling rate set by the user, which for these tests was 1 MHz.

V. Data Analysis

Five 8-ms time samples are used for an ensemble average of the data. These data are measured by the Kulite transducer mounted in the base of the forward-facing cavity. Each 8-ms time block is taken after one pulse from the Nd:YAG laser. More samples were not used due to the time difference between the first and last trace. The conditions could vary greatly for longer lengths of time. For example, blunt models typically experience separation on the nozzle wall in the initial moments of the run. This may be due to a shock-boundary layer interaction, when a strong bow shock off of the model impinges on the nozzle wall. When separation occurs on the nozzle wall, the nozzle-wall boundary layer can sometimes experience reattachment. Data from before this separation occurs or after reattachment can be used. For quiet flow, after 2 seconds of run time or less, the freestream noise in the tunnel increases.[11] This noise increase is suspected to be related to noise increase in the contraction, which results from free convection currents. The tunnel conditions also change about every 0.2 seconds, when expansion wave reflection in the contraction of the BAM6QT reduces the stagnation conditions. Turbulent bursts also appear more frequently on the nozzle

wall for high-Reynolds-number runs. These turbulent bursts are random, but the Mach waves preceding the turbulent bursts can interact with the forward-facing cavity model (Figure 16 in[19]).

To determine the number of averages necessary for time traces and spectra, different numbers of averages were examined for a case where there were no turbulent bursts on the nozzle wall during a run. These are shown in Figure 7. Figure 7(a) shows that when more than 5 averages of fast Fourier transforms are taken, the spectra all appear to be fairly similar. Only slight changes to the noise floor are observed. Thus, it may be acceptable to take somewhere between 5 and 10 averages.

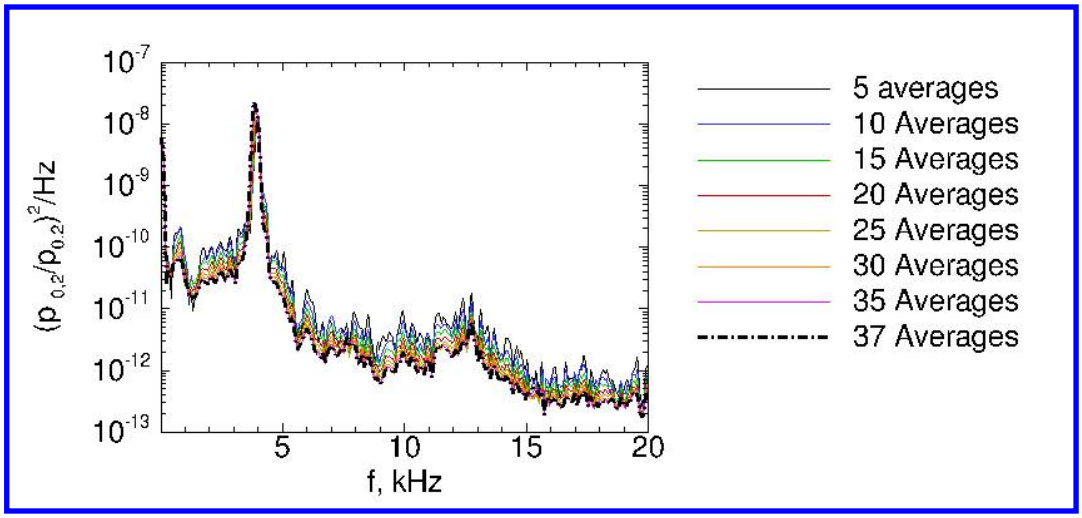

(a) 5 or more averages.

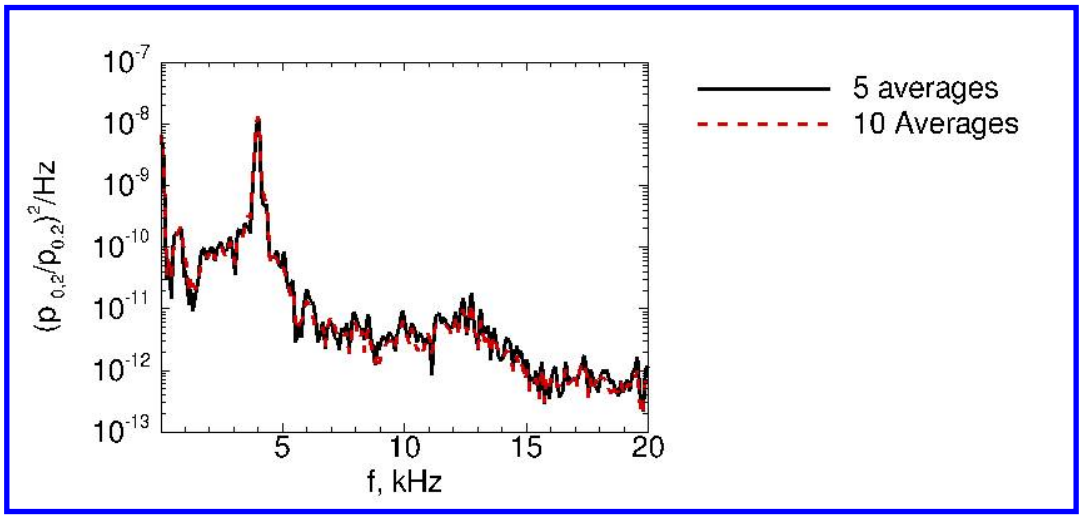

(b) 5 averages compared to 10 averages.

Figure 7. A comparison of the number of averages necessary to produce acceptable spectra. $L/D = 1.00$**,** $p_{0,1} \approx 1080$ **kPa,** $T_{0,1} \approx 428$ **K,** $M = 6.0$**.**

While it is desired to take more averages, this requires more laser pulses which are not affected by changes in conditions. At the high Reynolds numbers tested, it is difficult for this to be achieved without any turbulent bursts on the nozzle wall, separation on the nozzle wall, or increase in tunnel noise.[11] Thus, the constraint on the number of FFTs that must be averaged should be relaxed, if possible. Figure 7(b) shows spectra that look very similar, regardless of if 5 or 10 averages are taken. This indicates that perhaps only 5 FFTs need to be averaged to produce acceptable spectra.

This method was compared to that used by Casper in her glow perturber experiments. Casper uses 50 averages of a perturbation with a repetition rate of 200 Hz. The first and last average of Casper's data never saw more than a 0.5 s difference.[22] Since the Nd:YAG laser pulses at 10 Hz, only five pulses happen in a 0.5-second time frame. Furthermore, at high stagnation pressures, more turbulent bursts tend to be present,

so laser pulses affected by turbulent bursts are more common. These traces could not be used. Thus, the longest span between the first and last data that were averaged for these experiments was 0.7 seconds.

VI. Results

To show that this method of creating perturbations in the freestream works for the BAM6QT, the forward-facing cavity experiments of Ladoon were duplicated and compared. The measured frequency of the cavity resonance was checked and compared to theory. Damping experiments similar to the Mach-4 experiments were also conducted. As before, a laser perturbation was created in the freestream and allowed to convect downstream to interact with the forward-facing cavity model. Since the length scales in the BAM6QT are an order of magnitude larger than in the PQFLT, some changes in the results are to be expected.

A. Measured Frequency of Cavity Resonance

Previous measurements with no forced perturbations in the freestream showed good agreement between the theoretical and measured fundamental resonance frequency.[19] When no forced perturbations are present in the freestream, the fundamental cavity resonance frequency was found by taking power spectra of a 0.1-second time sample after the tunnel start time. The frequency of the largest-amplitude peak was then assumed to be the fundamental of the cavity resonance frequency.

When laser perturbations are present in the freestream, the resonance frequency was found by taking power spectra as described in Section V. Again, the largest-amplitude peak is taken to be the fundamental cavity resonance. Using the example spectra is given in Figure 7(b), the fundamental frequency of the cavity resonance is given by the large peak at about 3.9 kHz.

A comparison of measurements of the frequency with and without laser perturbations in the freestream is given in Figure 8. The red squares are measurements made by Ladoon in the PQFLT using a laser perturbation in quiet flow.[16] Measurements made in the BAM6QT are given by the blue open circles and green filled triangles. The blue open circle represents the fundamental frequency when there are no forced perturbations in the freestream (quiet flow). The green filled triangle shows the measured fundamental frequency when there are laser perturbations upstream of the cavity in quiet flow. These measured values are within 6% of the frequency predicted by Equation 2. The error likely stems from the approximation of the shock standoff distance δ. These data show that the resonance frequency is the same for cases with and without forced perturbations.

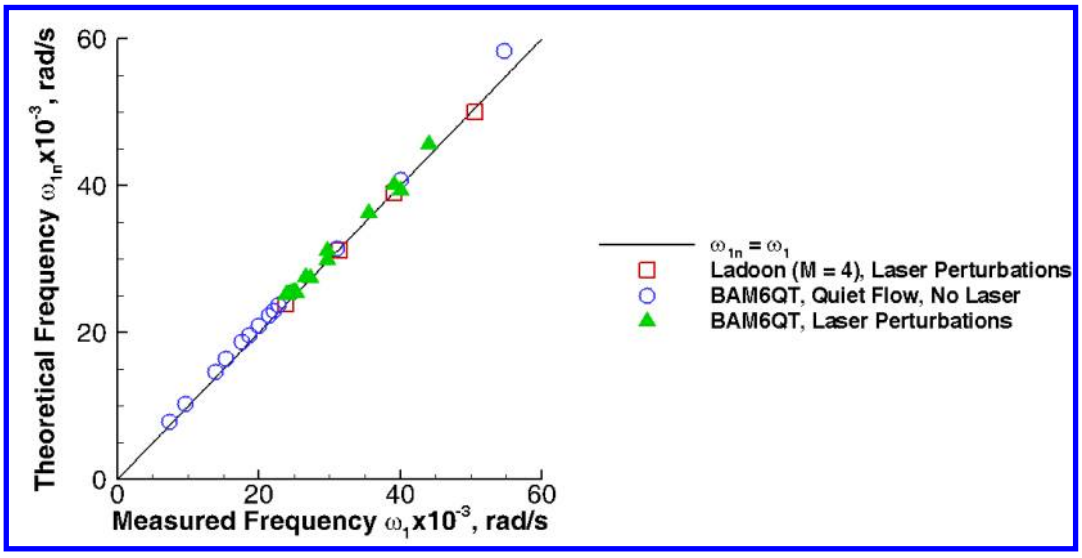

Figure 8. A comparison of measured and theoretical fundamental frequency of cavity resonance (Equation 2).

B. Maximum Distance for Detectable Laser Perturbation

In previous tests, when the model is placed farther downstream of the laser perturbation, the response was markedly decreased for unknown reasons. Initially, the forward-facing cavity was positioned so that $z_{\text{nose}} = 2.374$ m. This was the same location used for many pitot-probe measurements. However, at this location, the cavity pressure did not respond to the perturbation. This previous result may have been due to alignment issues, which are discussed in Reference 10. It is possible that the perturbation was not created on-axis with the forward-facing cavity model and therefore does not convect in a straight line toward the model when it is far downstream.

While the thermal perturbation is not expected to decay over such a short distance, this possibility was tested. These experiments also served to find the maximum distance the model could be placed from the perturbation while still being able to detect the perturbation. To do this, the model is set with a cavity of $L/D = 1.00$, which is slightly less than the critical depth of the forward-facing cavity. The distance between the model and perturbation (Δz) was adjusted between each tunnel run. Perturbations were detected with this forward-facing cavity configuration up to a distance of $\Delta z/D = 27.3$ away. Farther distances were not tested. However, the response changed in both magnitude and character as the distance was increased.

To show how the forward-facing cavity response changes with distance from the laser perturbation, Figure 9 shows the individual traces and ensemble averages of the response. The cavity base pressure response for five different laser perturbations are given by light gray traces. The red traces show the ensemble average of these five samples. As the model is moved farther away, the response to the perturbation changes and the time that it takes the perturbation to cause a response changes. The closest location of $\Delta z/D = 3.15$ (Figure 9(a)) gives a damped sinusoidal shape, similar to what was seen by Ladoon.[16] However, at the next closest location of $\Delta z/D = 7.35$ (Figure 9(b)), the characteristic of the response changes. First, some high-frequency content appears in the ensemble-averaged trace. The cavity base pressure oscillations then begin to decay exponentially, as before. As the distance is increased, there appears only to be the high-frequency noise and the rest of the trace is similar to a case when there are no laser-generated perturbations in the freestream (Figure 10(b)).

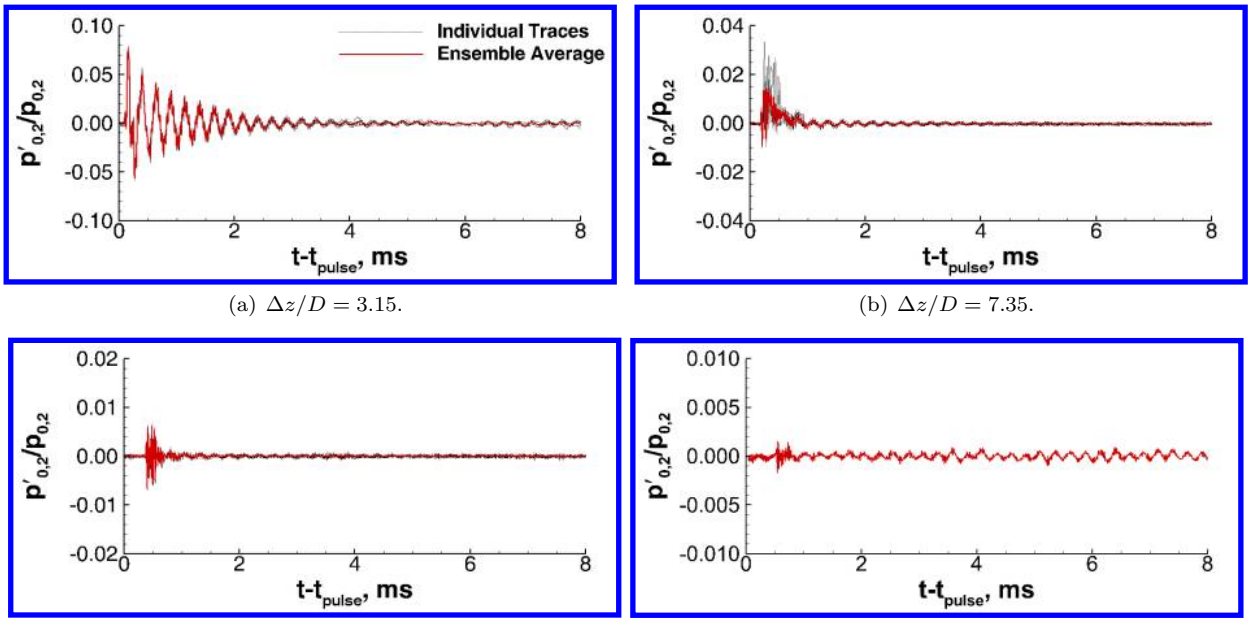

(a) $\Delta z/D = 3.15$.

(b) $\Delta z/D = 7.35$.

(c) $\Delta z/D = 16.8$.

(d) $\Delta z/D = 25.2$.

Figure 9. Cavity base pressure response for different model locations. $Re/m = 11.8 \pm 0.2 \times 10^6$**/m,** $L/D = 0.996$**. Note the changes in scale on the y-axis.**

Figure 10 shows time traces of the pressure fluctuations in the forward-facing cavity at one of the farthest aft measurement positions. Figure 10(a) shows the response of the cavity due to a laser perturbation. Figure 10(b) shows the response of the cavity when there is no laser perturbation. Figure 10(c) shows the electronic noise trace. These are not averaged time traces, because it was difficult to determine whether or

not "ensemble averages" of 8-ms blocks would be in phase when there was no forcing perturbation in the freestream. For comparison, the cases where there was a laser-generated perturbation in the freestream are also not averaged. Instead, Figure 10(a) shows a time trace taken after one laser pulse. Post-processing of these traces included low-pass filtering the traces with an 8-pole Butterworth filter at a frequency of 200 kHz. This trace was taken by exposing the Kulite sensor mounted in the model to a vacuum pressure of about 1.10 kPa. No flow was present in the tunnel at this time. The laser was turned on at full power, but with the laser beam blocked with a beam stopper placed in front of the tunnel windows. The fluctuations recorded by the Kulite were then normalized using the total pressure used in Figure 10(a).

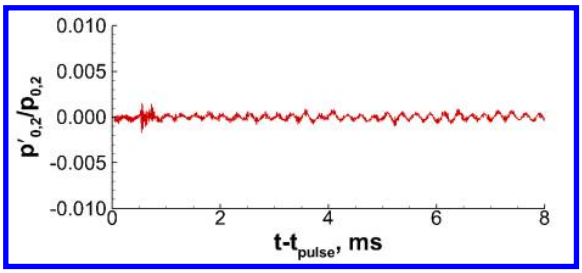

(a) Laser perturbation in freestream. $\Delta z/D = 25.2$.

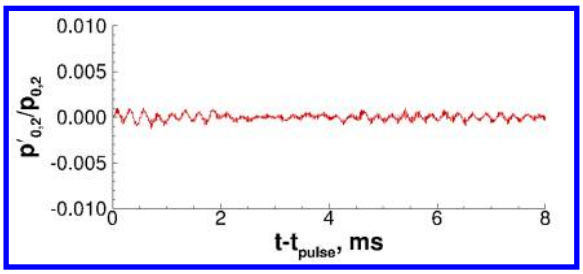

(b) No laser perturbations. $\Delta z/D = 25.2$..

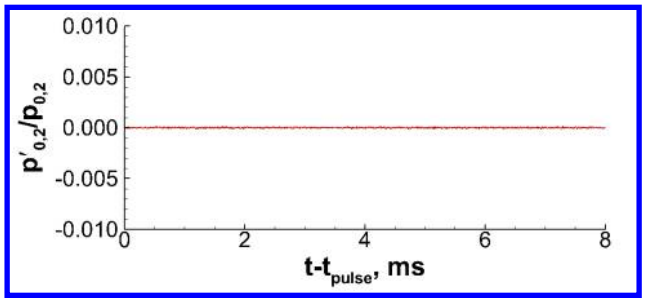

(c) Electronic noise.

Figure 10. Cavity base pressure response for different model locations. $Re/m = 11.8 \pm 0.2 \times 10^6$**/m,** $L/D = 0.996$**.**

It was previously thought that the forward-facing cavity was responding to the thermal disturbance. However, it is possible that it is responding to the weak acoustic disturbance instead. At the farther locations, the acoustic disturbance may have begun to dissipate and may not be causing as large a response. The magnitude of the maximum overshoot in response is plotted against the location of the model in the tunnel in Figure 11. This maximum pressure response appears to decay exponentially with distance.

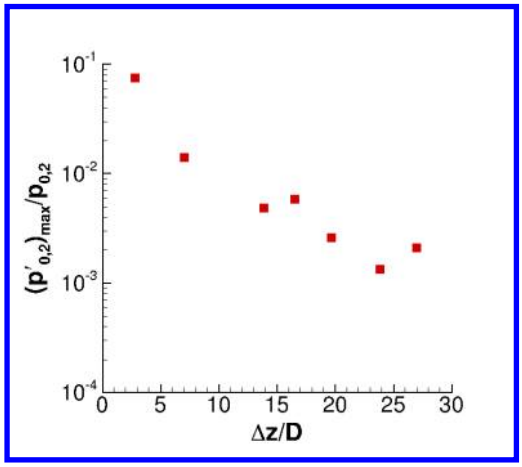

Figure 11. Maximum pressure response due to laser perturbation for each streamwise position of the forward-facing cavity tested.

To better determine whether the acoustic or the thermal disturbance is generating the cavity response,

the speed of the disturbance can be used. The response time (t_r) will be taken as the time between when the laser pulse is fired and when the cavity base pressure response reaches 10% of the maximum response. This response time to the perturbation can be plotted against the distance to the cavity nose (Δz) in order to find the speed of the disturbance. The unfiltered traces are used for this analysis in order to ensure that no phase lag exists between each of the traces used. The average of five time traces at each of these locations is used.

Figure 12 shows the cavity base pressure response when the model is placed at different distances from the perturbation. Each pressure trace is offset by an amount proportional to the distance downstream from the perturbation's initial location, $z = 1.925$ m. From this figure, it appears that there is a fairly linear relationship between the model location and the time at which the Kulite measures a response.

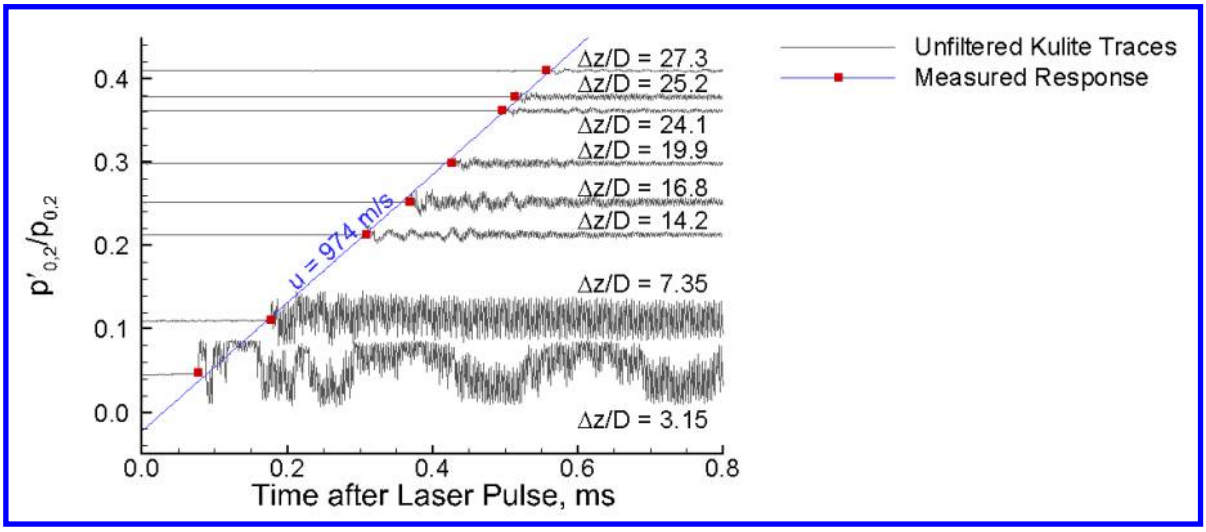

Figure 12. Cavity base pressure response for different model locations. $L/D = 1.00$, $M_\infty = 6.0$, $p_0 = 1074$ kPa, $T_0 = 426$ K, $E_{\text{pulse}} = 160$ mJ/pulse.

The distance between the cavity nose and perturbation (Δz) was then plotted against the response time (t_r) and a least-squares fit was applied. This provided a linear fit with the following equation:

$$\Delta z = 974\frac{\text{m}}{\text{s}} \cdot t_r - 0.0279\,\text{m} \tag{5}$$

$$= 974\frac{\text{m}}{\text{s}}\,(t_r - 28.6\mu\text{s}) \tag{6}$$

From this linear fit, it appears that the speed of the perturbation is about 974 m/s. There also appears to be some offset between when or where the perturbation is created and when the Kulite sensor responds to be perturbation. This offset is a distance of 2.79 cm or a time delay of 28.6 μs or some combination of the two. The response time t_r is measured relative to when a laser pulse is fired. The cause of this delay is unknown.

At the conditions where these measurements were made, the speed of sound is about 144 m/s. The thermal perturbation is expected to be flow-fixed, or to travel with the freestream speed,[3] which is about 867 m/s. The fastest the acoustic disturbance can travel is about 1011 m/s. This number is only 3.7% different from the measured speed of the disturbance. So, from this, it is likely that the acoustic disturbance is generating the ringing response in the forward-facing cavity. Any differences may be from the assumed static temperature of 52.0 K and assumed Mach number of 6.0. As mentioned previously, the model sits far forward at some of these measurement locations, in a region where the flow may not be uniform.

It is difficult to pinpoint when or if other parts of the perturbation affect the cavity base pressure. At locations where $\Delta z/D$ is small, the expected arrival of the thermal perturbation occurs very soon after the fast acoustic perturbation. This makes it difficult to distinguish between the response of the Kulite pressure transducer to each component of the laser perturbation. Linear and nonlinear interactions may occur due to the response of the model to the different types of perturbations and this may cause the data to be unclear. Damping of the first portion of the laser-generated perturbation (fast acoustic wave) may not occur

fast enough to clearly see the response of the second portion of the laser-generated perturbation (thermal perturbation).

C. Damping Characteristics

Damping characteristics for the forward-facing cavity were examined for $L/D = 0.00$–1.00 at Mach 6. Only data from the farthest forward location was used for this analysis because this distance is similar to the separation between the model nose and initial perturbation location used by Ladoon.[16] Thus, the perturbation is likely to be similar to that used by Ladoon.

Pressure traces were taken after five different laser pulses and averaged to form a representative trace. An example of the average of these traces and the exponential envelope fit to the averaged trace is given in Figure 13. The red line is the ensemble-averaged trace, and this is the trace used in determining the best exponential envelope fit. The dashed black line is the exponential fit, which is found by using a least-squares fit to the peaks of the red pressure trace.

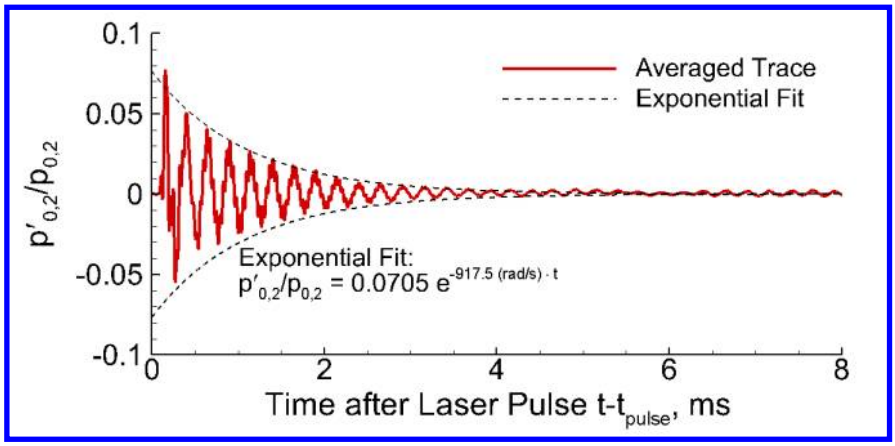

Figure 13. Example of averaged pressure traces. $L/D = 1.00$, $p_{0,1} = 1050.3$ **kPa,** $T_0 = 153.4°$**C,** $M_\infty = 6.0$, $E_{\text{pulse}} = 179.6$ **mJ/pulse, quiet flow.**

1. *Damping of Cavity Resonance and Resonance Frequency*

The damping coefficients were plotted against their corresponding fundamental frequencies for a comparison to Ladoon's prediction. The best power-law fit to the data at Mach 6 was:

$$\frac{\gamma}{2} = 3.54 \times 10^{-11}\,\omega_1^{3.03}. \tag{7}$$

The amplitude constant for this fit is an order of magnitude larger than that in Ladoon's power-law fit (Equation 4). As shown in Figure 14, the data fall on two separate curves. This indicates that some difference between the two experiments affects the damping. Thus, the damping coefficient cannot be scaled simply by comparing ω_1.

Many parameters change between Ladoon's experiment and the present BAM6QT experiment. Some of these parameters are listed in Table 1. How these parameters affect the physics of the cavity flow is unknown. Furthermore, the Mach-6 tests were conducted with the model far forward in the tunnel, in a region with non-uniform flow. This may also affect the damping of the cavity resonance.

Ladoon's data consistently shows about an order of magnitude slower damping than the data found in the BAM6QT. This is further illustrated in Figure 15, where the averaged pressure trace for data in the BAM6QT with a similar ω_1 can be compared to the pressure trace from Ladoon's work. Figure 15(a) shows a signal that appears to take four times longer to decay than the signal in Figure 15(b). This suggests that the parameter ω_1 is dependent on some parameter that changes between the PQFLT experiment and the BAM6QT experiment.

However, using Equation 7, the critical depth can still be estimated using only the data collected at Mach 6. For the case where $\omega_1 = 25200$ rad/s, Equation 7 gives a decay rate of $\gamma/2 = 775$ rad/s. The slope of Equation 7 at $\omega_1 = 25200$ rad/s is then 0.0932. This gives that the critical resonance frequency

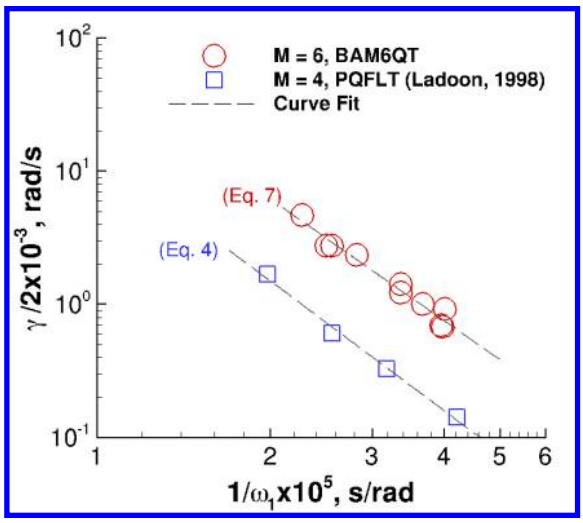

Figure 14. A comparison of damping coefficients for different cavity frequencies.

Table 1. Comparison of conditions in the PQFLT and the BAM6QT for forward-facing cavity experiments.

Condition	PQFLT[16]	BAM6QT
Freestream Mach Number, M_1	4	6
Freestream Stagnation Pressure $p_{0,1}$, kPa	100 ± 3	1050 ± 4
Stagnation Pressure Behind Shock $p_{0,2}$, kPa	13.9 ± 0.4	31.1 ± 0.1
Stagnation Temperature T_0, K	298 ± 3	426 ± 5
Stagnation Sound Speed a_0, m/s	346	417
Mean Bow Shock Standoff Distance δ, mm	3.7	6.5
Cavity Diameter D, mm	9.53	19.05
Maximum Cavity Depth Tested L, mm	18.91	18.98
Unit Reynolds Number Behind Shock Re_2/m, $\times 10^6$	1.22	1.65

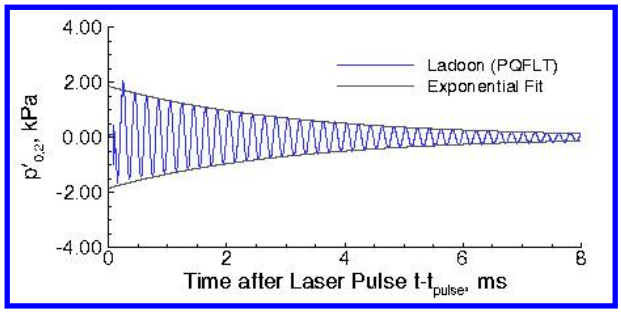

(a) PQFLT (Ladoon), $\omega_1 = 31400$ rad/s, $L/D = 1.426$. $Re_2/\text{m} = 1.22 \times 10^6/\text{m}$.

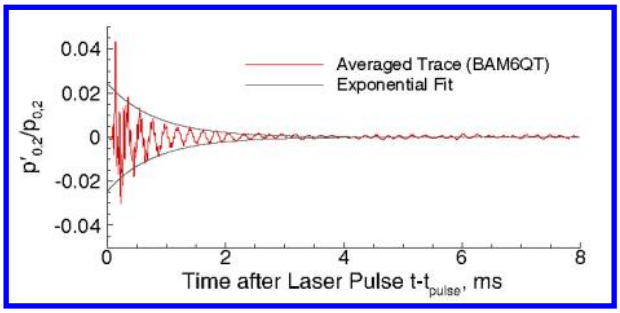

(b) BAM6QT, $\omega_1 = 29700$ rad/s, $L/D = 0.798$. $Re_2/\text{m} = 1.690 \times 10^6/\text{m}$.

Figure 15. A comparison of damping rates for cavities with similar ω_1.

$\omega_{1,\text{critical}} = 16900$ rad/s. Using Equation 2, the critical resonance frequency can be related to the cavity depth. A representation of Equation 2 that gives the critical nondimensional cavity depth can be expressed as

$$\left(\frac{L}{D}\right)_{\text{critical}} = \frac{\pi a_0}{2D\omega_{1,\text{critical}}} - \frac{\delta}{D} \tag{8}$$

Assuming that $a_0 = 417$ m/s, this gives that $(L/D)_{\text{critical}} = 1.70$. The critical cavity depth found using this

method of extrapolation is closer to the value found experimentally than Ladoon's estimate of $(L/D)_{\text{critical}} = 2.7$. A critical cavity depth of $L/D = 1.2$ was found in previous experiments.[19] However, the extrapolated value of $(L/D)_{\text{critical}} = 1.70$ is still 41% different from the value found experimentally.

2. *Damping of Cavity Resonance and Cavity Depth*

Another way of looking at the data was to analyze the relationship between the damping constant and the cavity depth. Figure 16 shows that cavity resonance in similar non-dimensional cavity depths decays in about the same amount of time. The damping for Ladoon's case in Figure 16(a) was $\gamma/2 = 611.2$ rad/s for $L/D = 1.064$. At $L/D = 0.996$ in the BAM6QT, the damping constant was $\gamma/2 = 917.5$ rad/s. These numbers are at least the same order of magnitude.

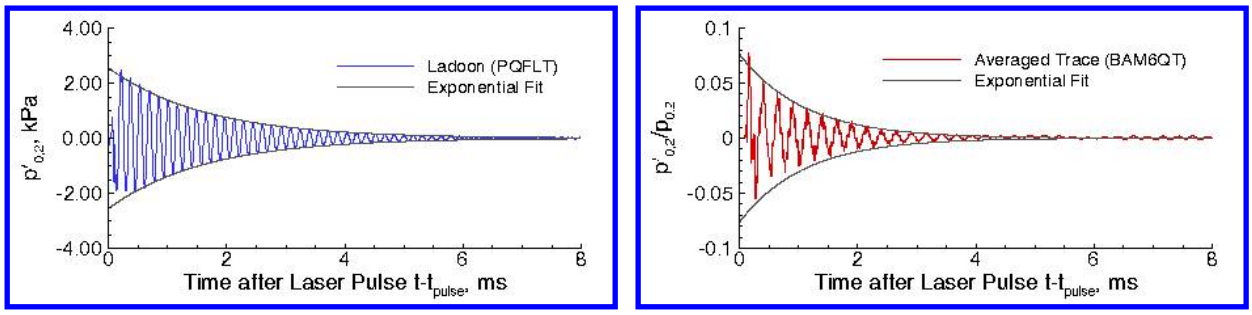

(a) PQFLT (Ladoon), $L/D = 1.064$. $Re_2/\text{m} = 1.22 \times 10^6/\text{m}$.

(b) BAM6QT, $L/D = 0.996$. $Re_2/\text{m} = 1.65 \times 10^6/\text{m}$.

Figure 16. A comparison of damping rates for cavities with similar L/D.

The data were plotted and a power law was fit to both sets of data from the PQFLT and BAM6QT. This is shown in Figure 17. The fit to the data is

$$\frac{\gamma}{2} = 725.7 \left(\frac{L}{D}\right)^{-2.130} \tag{9}$$

and has a coefficient of determination (R^2) of 0.982. This implies a correlation between the non-dimensional cavity depth and the damping coefficient that is independent of the parameters listed in Table 1. Thus, it seems appropriate to compare the decay rates found in different tunnels using the non-dimensional quantity L/D rather than the angular frequency of cavity resonance (ω_1).

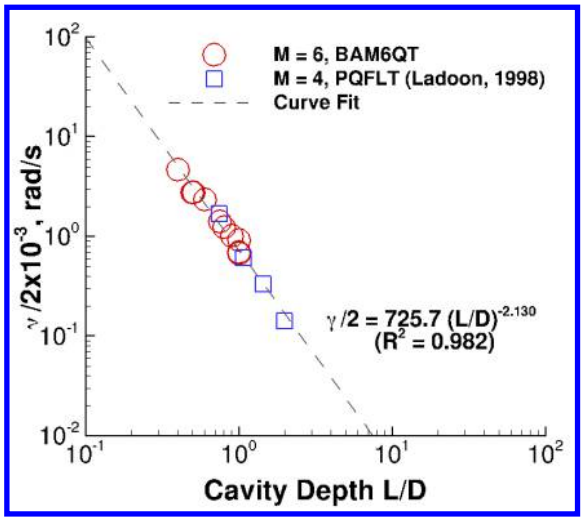

Figure 17. Power law fit for data from PQFLT and BAM6QT.

The use of this power law to find the critical cavity depth, however, still does not work well. Using only the data taken at Mach 6, the point with the longest decay time occurs at $L/D = 0.996$. Equation 9 gives a

decay rate of 731.9 rad/s. The slope of Equation 9 at $L/D = 0.996$ is found to be about 1566 rad/s. A linear extrapolation of the data gives that the critical depth $L/D_{\text{crit}} = 1.46$. This number is closer than both the value calculated by Ladoon[16] and the value calculated using Equation 7. However, it is still 22% different from the measured critical depth.

VII. Summary

The forward-facing cavity is used to verify the effectiveness of the laser perturber apparatus. This model has a well-known response, which has been explored in previous computations and experiments. The forward-facing cavity resonance appears to be initiated by the acoustic disturbance that results from the laser-generated perturbation. As the distance from the perturbation is increased, the response to the perturbation decreases. Damping characteristics of the forward-facing cavity were also examined. Cavities with the same resonant frequency damp almost an order of magnitude faster in the Mach-6 tunnel than they do in the former Mach-4 tunnel. However, resonance in cavities with the same non-dimensional cavity depth L/D appear to dampen at the same rate. This could provide information to help design future geometries with a forward-facing cavity configuration.

Acknowledgments

This research was funded by AFOSR Grant FA9550-12-1-0167 and an NDSEG Fellowship. Also, the authors would like to thank Chris Ward for his help in providing data on the axial displacement of the tunnel during a run.

References

[1]S. P. Schneider. Development of hypersonic quiet tunnels. *Journal of Spacecraft and Rockets*, 45(4):641–664, Jul–Aug 2008.

[2]S. P. Schneider. Effects of high-speed tunnel noise on laminar-turbulent transition. *Journal of Spacecraft and Rockets*, 38(3):323–333, May–Jun 2001.

[3]J. D. Schmisseur. *Receptivity of the Boundary Layer on a Mach-4 Elliptic Cone to Laser-Generated Localized Freestream Perturbations*. PhD thesis, School of Aeronautics & Astronautics, Purdue University, West Lafayette, IN, Dec 1997.

[4]T. R. Salyer, S. H. Collicott, and S. P. Schneider. Characterizing laser-generated hot spots for receptivity studies. *AIAA Journal*, 44(12):2871–2878, Dec 2006.

[5]J. D. Schmisseur, S. H. Collicott, and S. P. Schneider. Laser-generated localized freestream perturbations in supersonic and hypersonic flows. *AIAA Journal*, 38(4), Apr 2000.

[6]S. H. Collicott. Initial Mach 6 LT spot maker design summary. Technical report, Aug 2010. Informal design report.

[7]J. Trolinger, J. Abiss, and R. Nichols. A generalized approach to selecting, designing, and constructing conformal optical windows for wind tunnels: Parts and components list. Technical report, MetroLaser, Inc., Irvine, CA, Oct 2002. Contract No. F40600-99-C-0015.

[8]P. Garrett and D. L. Weber (Dynamic Engineering Incorporated). Engineering drawings, Mar 2002. Drawing Numbers 922–61, 922–62, 922–63.

[9]D. Weber (MetroLaser). Private communication, Jan 2002.

[10]D. C. Berridge, C. A.C. Ward, R. P.K. Luersen, and A. Chou. Boundary-layer instability measurements in a Mach-6 quiet tunnel. AIAA Paper 2012-3147, Jul 2012.

[11]L. E. Steen. Characterization and development of nozzles for a hypersonic quiet wind tunnel. Master's thesis, School of Aeronautics & Astronautics, Purdue University, West Lafayette, IN, Dec 2010.

[12]W. A. Engblom, D. B. Goldstein, D. W. Ladoon, and S. P. Schneider. Fluid dynamics of hypersonic forward-facing cavity flow. *Journal of Spacecraft and Rockets*, 34(4):437–444, Jul–Aug 1997.

[13]L. D. Huebner and L. R. Utreja. Mach 10 bow-shock behavior of a forward-facing nose cavity. *Journal of Spacecraft and Rockets*, 30(3):291–297, 1993.

[14]R. N. Hopko and K. H. Strass. Some experimental heating data on convex and concave hemispherical nose shapes and hemispherical depressions on a 30° blunted nose cone. Technical report, Mar 1958. NACA RM L58a17a.

[15]R. L. Stallings and P. B. Burbank. Heat-transfer and pressure measurements on a concave-nose cylinder for a mach number range of 2.49 to 4.44. Technical report, Oct 1959. NACA TM X-221.

[16]D. W. Ladoon, S. P. Schneider, and J. D. Schmisseur. Physics of resonance in a supersonic forward-facing cavity. *Journal of Spacecraft and Rockets*, 35(5):626–632, Sep–Oct 1998.

[17]T. J. Juliano, R. Segura, M. P. Borg, K. M. Casper, Jr. M. J. Hannon, B. M. Wheaton, and S. P. Schneider. Starting issues and forward-facing cavity resonance in a hypersonic quiet tunnel. AIAA Paper 2008-3735, Jun 2008.

[18]Rodrigo Segura. Oscillations in a forward-facing cavity measured using laser-differential interferometry in a hypersonic quiet tunnel. Master's thesis, West Lafayette, IN, Dec 2007.

[19]C. A.C. Ward, B. M. Wheaton, A. Chou, R. P.K. Luersen, L. E. Letterman, and S. P. Schneider. Hypersonic boundary-layer transition research in the Boeing/AFOSR Mach-6 Quiet Tunnel. AIAA Paper 2012-282, Jan 2012.

[20]H. W. Liepmann and A. Roshko. *Elements of Gasdynamics*. Wiley, New York, 1957.

[21]S. P. Schneider, C. Skoch, S. Rufer, S. Matsumura, and E. Swanson. Transition research in the Boeing/AFOSR Mach-6 Quiet Tunnel. AIAA Paper 2002-0302, Jan 2002.

[22]K. M. Casper, S. J. Beresh, and S. P. Schneider. Pressure fluctuations beneath turbulent spots and instability wave packets in a hypersonic boundary layer. AIAA Paper 2011-0372, Jan 2011.